Fluorescence Microscopic Imaging and Image Analysis of the Cytoskeleton

Gerlind Herberich[1], Thomas Würflinger[1], Antonio Sechi[2], Reinhard Windoffer[3], Rudolf Leube[3] and Til Aach[1]
Email: gh@lfb.rwth-aachen.de
[1]Institute of Imaging and Computer Vision, RWTH Aachen University, Germany
[2]Institute of Biomedical Engineering, University Hospital Aachen, Germany
[3]Institute of Molecular and Cellular Anatomy, University Hospital Aachen, Germany

***Abstract*—Cell stability and motility depends on a complex dynamic cytoplasmic scaffolding called the cytoskeleton. It is composed of actin filaments, intermediate filaments and microtubules, and interacts with neighbouring cells and the extracellular matrix via specialized adhesion sites - multimolecular complexes responsible for the transmission of mechanical force and regulatory signals. The dynamic behaviour of these subcellular structures in living cells can be analysed by fluorescence microscopy yielding series of 2D or 3D images. Towards a quantitative analysis, we present methods for the segmentation and motion estimation of cytoskeletal filaments as well as for the tracking of adhesion sites, allowing the quantification of cytoskeletal dynamics under different conditions.**

I. Introduction

The cytoskeleton (Fig. 1) consists of a complex intracellular scaffolding that is composed of protein fibers referred to as filaments. Based on their specific structural and functional properties three filament types are distinguished: actin filaments, intermediate filaments and microtubules. The cytoskeleton is a highly dynamic and adjustable scaffolding that is anchored to the surrounding extracellular matrix and to neighboring cells through distinct adhesion sites - multimolecular complexes that participate in the transmission of mechanical force and regulatory signals. The cytoskeleton is responsible for many basic cell functions such as mechanical resilience, motility (cell motion) and mitosis (cell division) and is involved in various disease processes. Cytoskeletal abnormalities frequently lead to disease. To better understand cytoskeleton-related diseases and to interfere with their pathophysiology, a precise knowledge of the plasticity of the cytoskeleton under different physiological and pathological conditions is crucial. The design and development of drugs capable of modulating the cytoskeleton in specific ways will therefore lead to new therapeutic agents. Cancer treatment provides prominent examples. Thus, by using anti-cytoskeletal (microtubule targeted) drugs one can efficiently interfere with the abnormally high division rate of cancer cells. This rational is the basis of some anti-cancer chemotherapeutic regimen today.

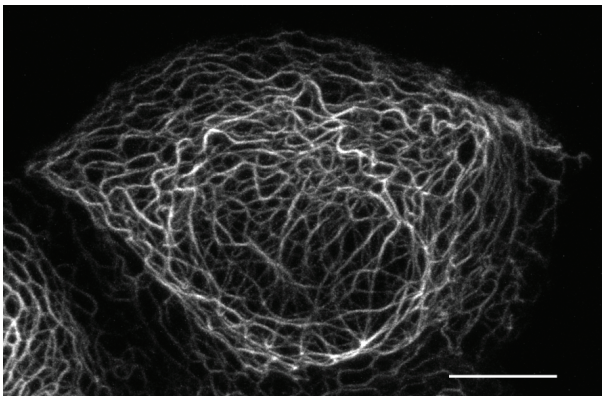

Fig. 1. Fluorescence microscopy of a cell producing fluorescent keratin intermediate filaments. The projection of 21 focal planes illustrates the dense filamentous network in the cytoplasm. Bar $10\mu m$.

Despite its importance for many human diseases, the cytoskeleton is still quite poorly understood. In order to better understand its dynamics, quantification of the filaments' shape, shape deformations and motion is essential. Highly reliable and reproducible quantification of these is only possible with an automated analysis of the filaments. Therefore, we acquired 2D and 3D image time-series of the cytoskeleton within living cells and developed methods for the automated analysis of these images. The tight coupling of imaging and image analysis is a matter of particular interest in this context as, due to the high diversity of biological processes, there are no standardized imaging protocols in fluorescence microscopy. Instead, the image acquisition parameters are optimized w.r.t the structure under investigation. In consequence, the image analysis methods have to deal with highly variable image data.

Related work includes Quantitative Fluorescent Speckle Microscopy by Danuser et al. [1] where speckles instead of filaments were analyzed. In [2], the dynamics of vimentin intermediate filaments were analyzed in 2D by a correlation-based block matching. Furthermore, there has been work on measuring the velocity of single actin filaments utilizing - after denoising - an active contour-based segmentation followed by a tracking algorithm [3]. None of these studies attempted the computation of a dense 3-dimensional displacement vector field to characterize the motion of both single filaments and filaments integrated into a network. In [4] (and slightly extended in [5]), a method for the segmentation of cytoskeletal filaments has been proposed which is based on a rotated matched filtering approach using a rod kernel of one-pixel width thereby

not accounting for the width of the sought structure. For the segmentation of line-like structures at the supracellular level, numerous approaches have been proposed, tailored towards applications such as vessel or neurite segmentation. See e.g. [6] for a comparison.

In this paper, we describe the image formation process, point out the characteristics of the image data and propose methods for the enhancement and analysis of such images. In particular, we introduce a method for the segmentation of microtubules, an approach for the tracking of focal adhesions and an algorithm for the estimation of a dense 3D motion field of keratin intermediate filament networks.

II. Fluorescence Microscopic Imaging of the Cytoskeleton and Preprocessing

Image time-lapse sequences of subcellular structures such as cytoskeletal filaments and focal adhesions within living cells can be acquired by labeling the proteins associated with the structure under investigation with a fluorescent protein. Then, the structure under investigation becomes visible under a fluorescence microscope while all other structures remain invisible. In the following, we will describe two common microscopy techniques for the acquistion of image data of fluorescent specimens: The wide-field fluorescence microscopy and the confocal laser scanning fluorescence microscopy for the acquisition of 2D images and 3D images respectively.

A. 2D Imaging: Wide-Field Microscopy

In wide-field microscopy, the whole specimen is illuminated at once and the excited fluorescence is captured by a CCD. The image data are therefore 2D projections of 3D specimens. They are often corrupted by high background fluorescence. Furthermore, the fluorescence intensity of the structure of interest may vary strongly. Especially in regions where many filaments form a dense network, they may exhibit a low intensity and in consequence a low contrast. To analyze the structures despite these difficulties, preprocessing is indispensable.

1) Preprocessing - Background Fluorescence Reduction and Contrast Enhancement: To eliminate the high background fluorescence, we calculate a background estimation and subtract it from the original image by Top-hat filtering. Furthermore, we want to enhance contrast in dense network regions. The filaments within such a region form a peak in the image's gray value histogram. Therefore, a histogram equalization systematically leads to an enhanced constrast in these regions.

B. 3D Imaging: Confocal Laser Scanning Microscopy

In a confocal laser scanning microscope (Fig. 2), a laser is focused by the optics onto a point within the specimen. The specimen starts to fluoresce at this point with a wavelength that is larger than the wavelength of the laser. Therefore the fluorescence is deflected at the beam splitter towards the detector - a photomultiplier tube. To mask fluorescence that originates from structures that are out-of-focus, an aperture is placed in front of the detector. In this way, the whole

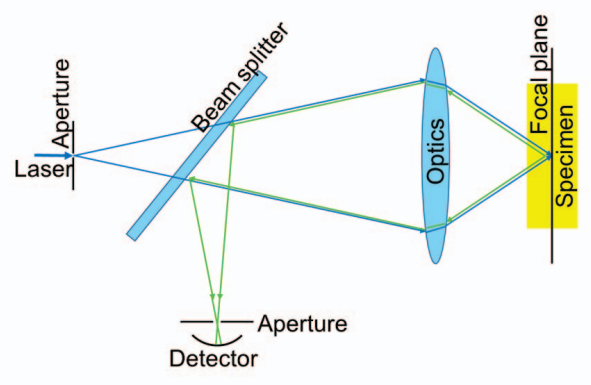

Fig. 2. Schema of confocal beam path.

focal plane is scanned point-wise yielding a 2D image which represents a section of the specimen. The focal plane is then moved to another depth of the specimen to acquire another slice such that in the end, the whole 3-dimensional structure of the specimen is imaged in a stack of such 2D slices which can be composed to a 3D image.

The two most important characteristics of such a 3D image are its spatial resolution and its SNR. The spatial resolution is highly anisotropic as the point spread function of a confocal laser scanning microcope limits the resolution along the optical axis much more than the resolution within the image plane: A voxel typically represents 60 nm in the dimensions of the 2D slices, and 500 nm in the dimension of the optical axis. In addition, due to the low fluorescence signal, the image data are strongly corrupted by photon counting noise.

1) Preprocessing - Poisson Noise Reduction: Photon counting noise is a Poisson process. For not too small counts, a Poisson distribution can be approximated by a signal-dependent Gaussian distribution. To get rid of the signal-dependence, we stabilize the variance by computing the Anscombe transform [7] such that the noise follows a Gaussian distribution with approximately constant variance.

Our goal is to preserve curvi-linear structures while reducing the noise. Curvelets [8], [9] are a sparse representation of such curvi-linear structures. After the curvelet transform, they are represented by a small number of large coefficients while the noise is not sparse in the curvelet domain and

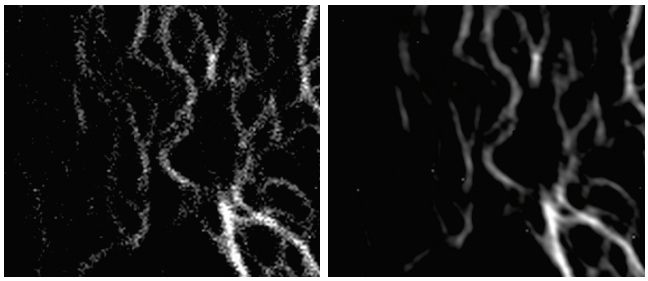

Fig. 3. Curvelet-based Poisson noise reduction: Original image of keratin intermediate filament network (left) and result of noise reduction (right).

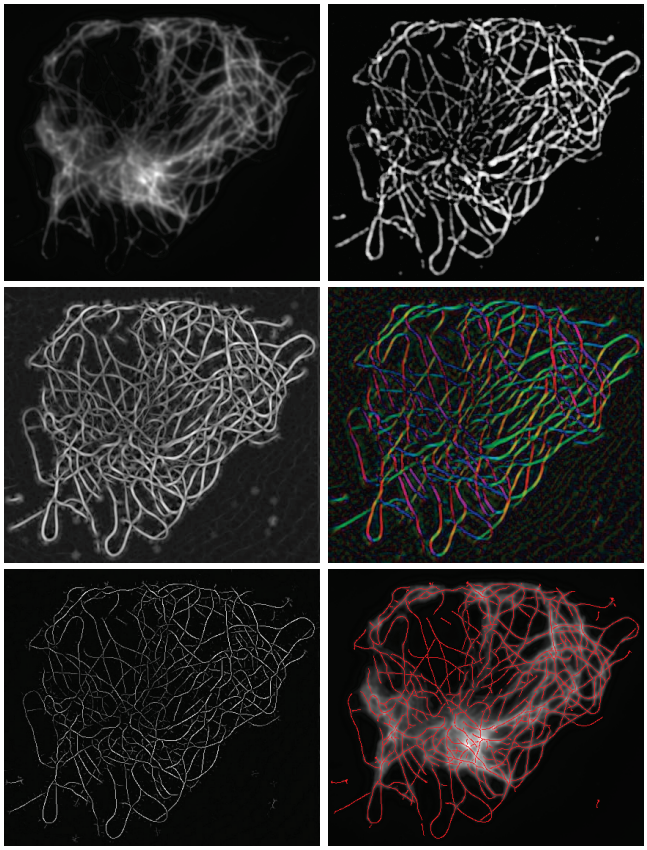

Fig. 4. Segmentation of microtubules in wide-field microscopic images. Top row: Original image (left) and result of preprocessing (right). Middle row: Ridge strength image (left) and orientation image (right). Bottom row: Result of nonmaxima suppression (left) and binary segmentation result (right) where red lines indicate the microtubules' centerlines.

therefore represented by a large number of small coefficients. In consequence, we can reduce the noise by thresholding the curvelet coefficients. As can be seen in the result (Fig. 3), the noise is significantly reduced while at the same time the filaments have not been blurred.

III. Image Analysis of the Cytoskeleton

This enhanced image data now forms the basis for our image analysis. In this section, we illustrate the methods we have developed for the analysis of cytoskeleton dynamics for wide-field (2D) and confocal (3D) microscopic images.

A. 2D Segmentation of Microtubules

Recently we have proposed a method for the segmentation of microtubules [10]. The goals of the segmentation are to first detect all microtubules despite their highly varying intensity and secondly to extract their centerline. The approach includes the preprocessing of wide-field data as described in section II-A1. The actual segmentation relies on a ridge detector which is built from derivatives of Gaussians [11]. To segment arbitrarily oriented ridges such as cytoskeletal filaments, we benefit from the steerability property of this ridge detector and

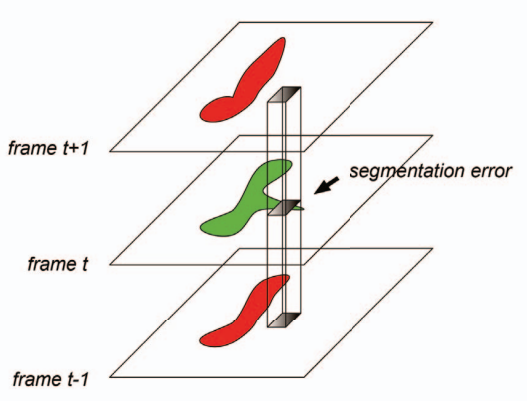

Fig. 5. Tracking of focal adhesions: Detection of segmentation errors for the spatio-temporal refinement of the segmentation [13].

analytically determine the ridge orientation which corresponds to the maximal ridge strength for each image point. In this way, we simultaneously obtain a ridge strength measure and an estimate of the ridge orientation. Towards extracting the microtubules' centerline, we thin the ridge strength image by suppressing nonmaxima [12]. To obtain a binary segmentation result, this thinned ridge strength image needs to be thresholded. As the high variability of the filaments' fluorescence is indeed significantly reduced after the preprocessing, but not completely eliminated, a simple threshold would reject all filaments from the final segmentation result that are dark in the original image and in consequence have a smaller ridge strength value than bright filaments. To keep these dark filaments despite their small ridge strength, we benefit from the fact that they are connected to filaments with a larger ridge strength. A hysteresis threshold then preserves the connectivity and leads to a satisfactory binary segmentation. Fig. 4 gives an overview of the different steps in the segmentation.

B. 2D Tracking of Focal Adhesions

In [13], [14] we have proposed an algorithm for the tracking of focal adhesions (FAs) in wide-field microscopic images. It achieves a large number of consistently tracked FAs due to the correction of segmentation errors during tracking. The algorithm consists of eight processing steps which we will briefly summarize in the following.

1) Foreground segmentation: The cytoplasmatic fluorophore pool is removed from the image by Top-hat filtering (see section II-A1) thus enabling the segmentation of FA population from the background by threshold segmentation using a threshold of 2.75% of the time series' maximal intensity.

In the following, adjacent, erroneously merged FAs are separated by applying a splitting step, which leads to an oversegmentation, and subsequently merged by incorporating a-priori knowledge about FA shape.

2) Splitting: Each connected component is treated as one hypothetical FA cluster. It is split up into potential individual FAs by subtraction of paths formed by pixels of near-

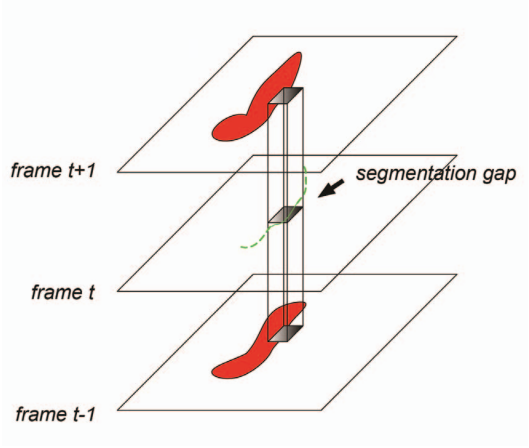

Fig. 6. Tracking of focal adhesions: Segmentation gaps in the course of time are first tolerated by the algorithm and closed in a later processing step [13].

background intensity. As only separating paths are of interest, the obtained hypothesised background regions undergo a morphological skeletonisation operation.

3) Model-based merging: Subcomponents that are part of individual FAs are detected using a geometric FA model and subsequently merged.

In the following four processing steps, the conditions for establishing the temporal context and refining the segmentations are set up:

4) Temporal object linking: The data exhibit a sufficiently high frame rate while the velocity of the FAs is low. Thus segmented objects in adjacent time frames I_t and I_{t+1} can be linked by an overlap criterion. Yet, such a criterion can easily be misled by segmentation errors in individual frames. Thus the algorithm must first be tolerant against gaps in the course of time (Fig. 6) and close them later on, deciding which segmentation was correct and which was not. In the case of gap frames, where no link is found, the algorithm is simply resumed on the next adjacent time frame I_{t+2}. The number of allowed successive gap frames was set to 6. The result of the linking is a set of linked lists of objects, each list being a hypothesis of a moving FA, stored along with the number of frames from its first appearance until its last detection.

5) Gap closure 1: Taking list length as a confidence measure, correct segmentations dominate over incorrect ones and close their gaps by appropriate reassignment of pixels using a highest-confidence-first strategy.

6) Segmentation refinement: Each FA segmentation can now be individually refined within a spatio-temporal, i.e. pseudo-volumetric neighbourhood (Fig. 5).

7) Gap closure 2: In the last processing step of the tracking, object shapes are carefully smoothed along time to further minimise segmentation inaccuracies and close remaining gaps, and segmentation dropouts are closed.

8) Measurements: The last step of the algorithm calculates FA parameters such as area, integrated fluorescence, elongation, orientation and velocity. At this stage either data from the whole FA population or from FAs within regions of interest can be collected. As analyses are carried out on the original images containing background fluorescence, an object-individual background correction is performed for the measurement of integrated fluorescence.

For the evaluation of the proposed algorithm on a time-series of 50 frames, an expert has generated a ground truth segmentation using ITK SNAP [15] of five representative FAs, which differed in size, brightness and cellular location. Features such as FA area, integrated fluorescence and elongation have been compared to the automatically computed results yielding very similar curves [13], [14].

C. 3D Motion Analysis of Keratin Intermediate Filaments

In this subsection, we present a method for the estimation of a dense 3D motion field of keratin intermediate filament networks using 3D image time sequences obtained from a confocal laser scanning microscope. The goal is to determine the local filament velocity for each image point.

First, to enhance the data, Poisson noise is reduced according to section II-B1. Before we can measure local filament motion we have to compensate for a global cell motion that superimposes the sought local filament motion. To this end, we register all frames using a rigid pre-registration algorithm. Then, we estimate the local filament motion. To avoid problems with the discrete approximation of partial derivatives in the presence of such a low spatial resolution in the third dimension of the image data our approach is a deformable registration algorithm. The criterion for the motion estimate can be written as a maximum-a-posteriori estimate.

To determine the data term, we verified that the assumption of brightness constancy holds for the temporal sampling of the data. Under the assumption that the pool of fluorescently labeled keratins in a single cell is stable, i.e. protein biosynthesis does not take place under the experimental conditions, the evolution of the integral fluorescence over time indicates bleaching of the fluorescently labeled keratins. The mean bleaching per pixel then provides a clear measure to determine whether a matching process may be based on the assumption of brightness constancy or whether bleaching effects have to be taken into account. Therefore we have computed the integral fluorescence per frame in a time series monitoring a single cell. The difference of the integral fluorescence between two consecutive frames represents a measure for the overall bleaching during the time interval dt between the two frames and the mean difference per pixel between two consecutive frames indicates the mean bleaching per pixel occured during dt. The mean bleaching per pixel for the whole time-series turned out to be $m = 0.556$. This results clearly shows that the brightness decrease does not play a role in a matching process based on quantized intensity values. We may thus assume brightness constancy.

Under the assumption that the remaining noise in the images exhibits a Gaussian distribution, a suitable data term then is the well known sum of squared differences (SSD). As regularization term, we choose an elasticity model to describe

the possible deformations of the filaments and thus enforce the resulting motion field to be C^0-continuous. Keeping in mind the huge amount of data that has to be processed, efficiency is an important aspect for our algorithm. Therefore, we superimpose a deformation grid on the image and estimate the motion only at the grid points. A subsequent interpolation then yields a dense 3D motion field (see [16] for details). In addition, we reformulate the MAP-criterion in terms of a labeling problem so that it can be optimized with a discrete optimization algorithm [17].

To evaluate the precision of our method, we have generated synthetic data by applying known motion fields to real image data: For the generation of the known motion fields, the image is first thresholded using the Otsu threshold [18]. The areas of the mask then correspond to image areas with significant structures. A deformation grid is superimposed to the image. The grid points contained within the mask are assigned vectors of random orientation and random length up to $1\mu m$. To generate a dense motion field from the random vectors, we apply a linear interpolation. The synthetic target image is then produced by warping an image using the synthetic motion field and then corrupting it with Poisson noise. The noise has a standard deviation $\sigma = sqrt(\lambda)$ with λ being the measured intensity. Our synthetic sequence consists of 70 frames. As error measure, we compute the endpoint error as the difference vector between ground truth motion $\mathbf{v}_{gt}$ and estimated motion $\mathbf{v}_{est}$: $\mathbf{v} = (v_x, v_y, v_z)^T = \mathbf{v}_{gt} - \mathbf{v}_{est}$. In optical flow evaluation [19] it is common to compute the mean magnitude of this difference vector. To evaluate the influence of the anisotropic spatial resolution on the estimation error, we calculate for each component the mean of its absolute value: $(\overline{|v_x|}, \overline{|v_y|}, \overline{|v_z|})^T = (38.3nm, 32.7nm, 67.1nm)^T$. This result clearly shows, that the method is subvoxel-precise and that as expected, the low resolution in the third dimension significantly aggravates the error vector magnitude.

IV. Summary and Conclusions

Imaging and image analysis of the cytoskeleton is a challenging, newly emerging field of research. We have illustrated two possibilities for the acquisition of images of the cytoskeleton within living cells. Then we have shown how this kind of image data can be enhanced. Finally, we have presented methods for the segmentation of microtubules and for the tracking of focal adhesions in wide-field microscopic data as well as an approach for the estimation of a 3D sub-voxel precise motion field of keratin intermediate filament networks in confocal microscopic data.

Interesting future prospects include the segmentation of the different kinds of branchings that appear in the cytoskeleton's network topology and the enhancement of the spatial resolution in confocal microscopic images. Another very important and yet challenging aspect is the reliable evaluation of segmentation as well as motion analysis results.

Acknowledgments

The work was supported in part by the German Research Council (WI 731/6-1) and by the excellence initiative of the German federal and state governments.

References

[1] G. Danuser and C. M. Waterman-Storer, "Quantitative fluorescent speckle microscopy of cytoskeleton dynamics." *Annu Rev Biophys Biomol Struct*, vol. 35, pp. 361–387, 2006.

[2] B. P. Helmke, D. B. Thakker, R. D. Goldman, and P. F. Davies, "Spatiotemporal analysis of flow-induced intermediate filament displacement in living endothelial cells." *Biophys J*, vol. 80, no. 1, pp. 184–194, Jan 2001.

[3] F. Raisch, H. Scharr, N. Kirchgener, B. Jaehne, R. Fink, and D. Uttenweiler, "Velocity and feature estimation of actin filaments using active contours in noisy fluorescence image sequences," in *Visualization, Imaging, and Image Processing - 2002*, 2002.

[4] N. Lichtenstein, B. Geiger, and Z. Kam, "Quantitative analysis of cytoskeletal organization by digital fluorescent microscopy." *Cytometry A*, vol. 54, no. 1, pp. 8–18, Jul 2003.

[5] S. A. Shah, P. Santago, and B. K. Rubin, "Quantification of biopolymer filament structure." *Ultramicroscopy*, vol. 104, no. 3-4, pp. 244–254, Oct 2005.

[6] S. Olabarriaga, M. Breeuwer, and W. Niessen, "Evaluation of hessian-based filters to enhance the axis of coronary arteries in ct images," in *Computer Assisted Radiology and Surgery*, ser. International Congress Series, H. Lemke, M. Vannier, K. Inamura, A. Farman, K. Doi, and J. Reiber, Eds., vol. 1256. London: Elsevier, June 2003, pp. 1191–1196.

[7] F. J. Anscombe, "The transformation of poisson, binomial and negative-binomial data," *Biometrika*, vol. 35, pp. 246–254, 1948.

[8] J.-L. Starck, E. Candes, and D. Donoho, "The curvelet transform for image denoising," *Image Processing, IEEE Transactions on*, vol. 11, no. 6, pp. 670 –684, Jun. 2002.

[9] B. Zhang, J. M. Fadili, and J.-L. Starck, "Wavelets, ridgelets, and curvelets for poisson noise removal," *IEEE Transactions on Image Processing*, vol. 17(7), pp. 1093–1108, 2008.

[10] G. Herberich, A. Ivanescu, I. Gamper, A. Sechi, and T. Aach, "Analysis of length and orientation of microtubules in wide-field fluorescence microscopy," in *Pattern Recognition, Proceedings of the 32nd DAGM*, vol. 6376. Springer, September 22–24 2010, pp. 182 – 191.

[11] M. Jacob and M. Unser, "Design of steerable filters for feature detection using canny-like criteria," *IEEE Transactions on Pattern Analysis and Machine Intelligence*, vol. 26, pp. 1007–1019, 2004.

[12] J. Canny, "A computational approach to edge detection," *IEEE Transactions on Pattern Analysis and Machine Intelligence*, vol. 8, pp. 679–698, 1986.

[13] T. Würflinger, I. Gamper, T. Aach, and A. S. Sechi, "Automated segmentation and tracking for large scale analysis of focal adhesion dynamics," *Journal of Microscopy*, 2010. [Online]. Available: http://dx.doi.org/10.1111/j.1365-2818.2010.03404.x

[14] T. Würflinger, A. S. Sechi, and T. Aach, "Segmentation, tracking, and analysis of focal adhesion dynamics in cellular microscopy imaging," in *IEEE International Conference on Image Processing (ICIP2009)*. Cairo: IEEE, November 7-11 2009, pp. 4209–4212.

[15] P. A. Yushkevich, J. Piven, H. C. Hazlett, R. G. Smith, S. Ho, J. C. Gee, and G. Gerig, "User-guided 3d active contour segmentation of anatomical structures: Significantly improved efficiency and reliability," *NeuroImage*, vol. 31, no. 3, pp. 1116 – 1128, 2006.

[16] G. Herberich, R. Windoffer, R. Leube, and T. Aach, "3D motion analysis of keratin filaments in living cells," in *Medical Imaging 2010: Image Processing*. San Diego, USA: SPIE Vol. 7623, February 13–18 2010.

[17] N. Komodakis and G. Tziritas, "Approximate labeling via graph cuts based on linear programming," *IEEE Transactions on Pattern Analysis and Machine Intelligence*, vol. 29, no. 8, pp. 1436–1453, 2007.

[18] N. Otsu, "A threshold selection method from gray-level histograms," *IEEE Transactions on systems, man, and cybernetics*, vol. SMC-9, pp. 62–66, 1979.

[19] S. Baker, D. Scharstein, J. P. Lewis, S. Roth, M. J. Black, and R. Szeliski, "A database and evaluation methodology for optical flow," in *ICCV*, 2007, pp. 1–8.